Supplemental Material

Subducted seamount diverts shallow slow slip to the forearc of the Northern Hikurangi Subduction Zone, New Zealand

Heather R. Shaddox[1] and Susan Y. Schwartz[1]

[1]Department of Earth and Planetary Sciences, University of California Santa Cruz, 1156 High Street, Santa Cruz, California, 95064 USA.

DATA AND METHODS

Hikurangi Ocean Bottom Investigation of Tremor and Slow Slip (HOBITSS) Network

The Hikurangi Ocean Bottom Investigation of Tremor and Slow Slip (HOBITSS) experiment deployed 24 absolute pressure gauges (APG) and 15 ocean-bottom seismometers (OBS) offshore of Gisborne, New Zealand from May 2014 - June 2015. Nine of the 15 deployed OBS stations returned data that can be used for time-sensitive analyses (EOBS 1-5, LOBS 1, 2, 6, and 8; Fig. 1). Two stations (LOBS 4 and 5; Fig. 1) did not return seismic data during the slow slip event, and four stations (LOBS 3, 7, 9, and 10; Fig. 1) have timing errors. Stations with timing errors are used in determining first-motion polarities, but do not contribute to the earthquake catalogs or template matching performed in this study.

Earthquake Locations

We use preliminary earthquake hypocentral locations and origin times from two earthquake catalogs compiled by J. Yarce (personal communication, 2018) and Todd et al. (2018). Both catalog's earthquakes were manually detected by picking P-wave and S-wave (where possible) arrivals at HOBITSS OBS stations and available land GeoNet seismic stations. The J. Yarce catalog includes events during the entire OBS deployment (May 2014 – June 2015). The Todd et

al. catalog focuses on events between September and October 2014, around the 2014 Gisborne SSE, and has more events during this time period than the J. Yarce catalog. We use 500 events from the Todd et al. catalog between September 1, 2014 and October 31, 2014, and 1,694 events from the J. Yarce catalog for the remainder of the study period (May 18, 2014 – August 31, 2014; November 1, 2014 – June 21, 2015), within the study region shown in Fig. 1. Preliminary hypocenters were found using Antelope's *dbgenloc* and *dblocsat2* algorithms. Hypocentral locations were then improved by relocating events with NonLinLoc v.6.0 (Todd et al., 2018) or BayesLoc (J. Yarce, personal communication, 2018).

To improve relative earthquake locations, we attempt to relocate the total 2,194 events (NonLinLoc and BayesLoc relocations) using GrowClust, a relative relocation algorithm that uses waveform cross-correlations (Trugman and Shearer, 2017). Cross-correlations are used to both determine waveform similarity and improve input differential travel times. GrowClust applies a hybrid, hierarchical clustering algorithm to both group and relocate events within similar clusters. Greater weight is given to event pairs with higher cross-correlations. This algorithm does not require explicit matrix inversion, improving stability, and uses the L1 norm so the results are less sensitive to input time outliers.

We use a local 1-D interpretation of the New Zealand 3-D velocity model (Eberhart-Phillips et al., 2010) centered offshore at -38.8361/178.4672 (Fig. DR3). This velocity model is not well constrained offshore. A comparison to the 1-D velocity model developed by Haijima, D. (2015) that uses both land and OBS stations for better offshore constraints is provided in Fig. DR3. For our study, the upper 10 km is of most interest because it is the depth range containing the clustered events above the subducted seamount that we interpret as occurring in the upper plate. The Eberhart-Phillips et al. (2010) velocity model has slower offshore seismic velocities above 3

km, then larger offshore seismic velocities until ~10 km compared to the Haijma model. Therefore, use of the Haijima 1-D velocity model in relocation would result in a deepening of the shallowest earthquakes (<3 km) and a shallowing of events in the 3-10 km depth range. These depth changes would move most of the "burst-type" repeating earthquake families farther from the plate interface and increase our confidence of their location within the upper plate fracture network above the subducted seamount.

Prior to performing waveform cross-correlations, traces are filtered using a 3-10 Hz 1 pass band-pass filter to remove noise on OBS stations below 3 Hz. For all event pairs, we compute cross-correlations for 0.6 seconds around the P-phase (0.2 second pre-pick) on the vertical channels. A maximum station distance of 100 km, a minimum average cross-correlation of 0.2 for each event pair, and a maximum root-mean-square (RMS) differential time residual of 0.3 s to join clusters are used for GrowClust parameterization. With these criteria, 773 of the input 2,194 events are relocated. Events not relocated lack waveform similarity, which is unsurprising given the scattered locations in the study area (Figs. DR1 and DR2) and sparse station coverage (even with the HOBITSS array). GrowClust implements a nonparametric resampling approach to estimate location uncertainties, allowing an assessment of the relocation results. Errors are median absolute deviations of the bootstrap distribution of hypocenter locations. Average horizontal and vertical location errors are 790 m and 720 m, respectively (Fig. DR2). Few events have final locations on the plate interface offshore. The clustered seismicity shown in Fig. DR2b where "burst-type" repeating earthquakes are found is located within the upper plate even considering the uncertainty in GrowClust locations. All 2,194 events, both GrowClust relocations and non-relocated Bayesloc and NonLinLoc locations, are shown in Figs. DR1 and DR2. A clustering of onshore events near the plate interface is evident in these figures, while offshore events are generally scattered within

the subducting slab. This onshore clustering and more scattered offshore locations was also found by Haijima, D. (2015) in a study that used OBS near the subducted seamount. We think that this feature reflects the different modes of strain release as a function of depth. In the offshore region, there are little to no underthrusting earthquakes on the plate interface and strain is released in slow slip events, while the deeper part of the plate interface beneath land does fail in underthrusting earthquakes. Therefore, this pattern likely develops due to differences in the frictional properties of the interface.

Template Matching

We use template matching to identify repeating earthquakes. We select template earthquakes from the GrowClust relocated earthquake catalog (773) as well the remaining 1,421 events not relocated with GrowClust. We are interested in events potentially related to the SSE. We therefore select events with final locations within 5 km of the plate interface in the general area of the SSE (Fig. DR1), for a total of 123 template events. Few of these potential plate boundary events are located within the modeled region of slow slip (slow slip >50 mm). Templates are generated and run two different ways to increase detections and account for emergent P-phase arrivals. The procedure is similar to that outlined in Igarashi et al. (2003).

The first set of templates are cut to five-second long windows around the P-phase arrival (0.15 second pre-pick). These templates often include the S-phase arrivals. Template events are then filtered using a 3-10 Hz zero-phase band-pass filter to minimize oceanic noise on the OBS stations. Template matching is performed on the vertical components. The second set of templates are clipped to two-second long windows around the S-phase (1 second pre-pick) to detect events with emergent P-phase arrivals. These template events are also filtered using a 3-10 Hz zero-phase band-pass filter and horizontal components are used.

Both sets of templates are scanned through continuous data between May 12, 2014 and June 20, 2015 using an open-source Python package, *EQCorrScan* (Chamberlain and Hopp, 2017). OBS stations are used because events are generally small ($<M_L$ 2) and poorly recorded on land stations. Further, the five EOBS stations (200 Hz sampling rate) have the highest signal-to-noise ratio and are predominantly used. For our study, a cross-correlation coefficient of greater or equal to 0.95 at a minimum of three or more stations is considered a repeating earthquake candidate. Figs. DR4 – DR7 give sample repeating earthquake seismograms. These are repeating earthquake candidates with high correlation-coefficients in the bandpass selected (3-10 Hz). Generally, events with this high level of similarity are located within one-quarter of the dominant wavelength (Geller and Mueller, 1980). The dominant frequency is 10 Hz (cut-off frequency used). Assuming a P-wave velocity of 4-5 km/s, the dominant wavelength is 400-500 m. Thus, any potential repeating earthquake pairs detected are likely less than 100-125m from each other.

Magnitude Estimation

We compute local magnitudes (M_L) for template events using the *Mlrichter* Antelope package, which is a computational class for computing M_L using magnitude and correction functions from Richter (1935). The correction values as a function of distance ($\log A_0$) established by Richter (1935) and applied in *Mlrichter* are based on observed shaking for southern California earthquakes. However, attenuation characteristics differ for New Zealand. We therefore edited the $\log A_0$ attenuation relationship for calculating M_L in the *Mlrichter* program based on the $\log A_0$ function for New Zealand earthquakes derived by Ristau et al. (2016), in which

$$\log A_0(R) = 0.29 - (1.27\times10^{-3})R - 1.49\log(R). \quad (1)$$

The resulting $\log A_0$ curve differs significantly from Richter (1935) at hypocentral distances (R) of less than 100 km and greater than 200 km.

We use the singular value decomposition (SVD) method presented by Rubinstein & Ellsworth (2010) to determine magnitudes of each earthquake within repeating earthquake families. We consider relative amplitudes, rather than moments, to compute the local magnitude of each repeating event based on the local magnitude of the template event, using the following relation:

$$M_L^i = \log_{10}\frac{A^i}{A^t} + M_L^t, \quad (2)$$

where A^i/A^t is the relative amplitude for the ith event, and M_L^t is the local magnitude for the template event.

We align the waveforms using cross-correlation prior to performing SVD analysis. To enhance signal to noise ratio (SNR) we apply a 3-10 Hz zero-phase bandpass filter. SVD analysis is computed used windows similar to what was used for template matching (i.e., either 5-second long windows with 0.15 second pre-pick relative to P-phase on vertical EOBS components or 2-second long windows with 1 second prior to S-phase on horizontal EOBS components). We require a cross-correlation of 0.85 at individual stations to compute SVD. Template and repeating earthquake detection magnitudes are included in Fig. 3 and Table DR1 (families near the subducted seamount).

Composite Focal Mechanisms

We are interested in the faulting geometry of the repeating earthquake families at the subducted seamount to determine whether these, like the SSE, occur on the plate interface. Since most of the earthquakes within a family are small ($M_L < 2$), first-motion polarities are generally only available at a few nearby stations. Therefore, rather than compute focal mechanisms, we determine whether the repeating earthquake families collocated with the subducted seamount are consistent with the geometry of the megathrust hosting the SSE. We take advantage of the high

similarity between repeating earthquakes in a family and stack waveforms at each station within a family to better determine P-wave first-motion polarities. Based on 4-6 available first-motion polarities for each family, nine of the eleven repeating earthquake families collocated with the subducted seamount are not consistent with underthrusting on the plate interface. The other three composite focal mechanisms are potentially consistent with the megathrust geometry.

REERENCES CITED

Chamberlain, C.J., and Hopp, C., 2017, EQcorrscan Documentation, v. 0.2.4:, https://media.readthedocs.org/pdf/eqcorrscan/latest/eqcorrscan.pdf (accessed August 2017).

Eberhart-Phillips, D., Reyners, M., Bannister, S., Chadwick, M., and Ellis, S., 2010, Establishing a Versatile 3-D Seismic Velocity Model for New Zealand: Seismological Research Letters, v. 81, p. 992–1000, doi:10.1785/gssrl.81.6.992.

Geller, R.J., and Mueller, C.S., 1980, Four similar earthquakes in central California: Geophysical Research Letters, v. 7, p. 821–824, doi:10.1029/GL007i010p00821.

Haijima, D., 2015, Seismic Activity and Velocity Structure in the Northern Hikurangi Subduction Zone offshore the North Island of New Zealand [M.S. thesis]: University of Tokyo.

Igarashi, T., Matsuzawa, T., and Hasegawa, A., 2003, Repeating earthquakes and interplate aseismic slip in the northeastern Japan subduction zone: Journal of Geophysical Research: Solid Earth, v. 108, doi:10.1029/2002JB001920.

Richter, C.F., 1935, An instrumental earthquake magnitude scale: Bulletin of the Seismological Society of America, v. 25, p. 1–32.

Ristau, J., Harte, D., and Salichon, J., 2016, A Revised Local Magnitude (ML) Scale for New Zealand Earthquakes: Bulletin of the Seismological Society of America, v. 106, p. 398–407, doi:10.1785/0120150293.

Rubinstein, J.L., and Ellsworth, W.L., 2010, Precise Estimation of Repeating Earthquake Moment: Example from Parkfield, California: Bulletin of the Seismological Society of America, v. 100, p. 1952–1961, doi:10.1785/0120100007.

Todd, E.K. et al., 2018, Earthquakes and Tremor Linked to Seamount Subduction During Shallow Slow Slip at the Hikurangi Margin, New Zealand: Journal of Geophysical Research: Solid Earth, v. 123, p. 6769–6783, doi:10.1029/2018JB016136.

Trugman, D.T., and Shearer, P.M., 2017, GrowClust: A Hierarchical Clustering Algorithm for Relative Earthquake Relocation, with Application to the Spanish Springs and Sheldon, Nevada, Earthquake Sequences: Seismological Research Letters, doi:10.1785/0220160188.

Wallace, L.M., Webb, S.C., Ito, Y., Mochizuki, K., Hino, R., Henrys, S., Schwartz, S.Y., and Sheehan, A.F., 2016, Slow slip near the trench at the Hikurangi subduction zone, New Zealand: Science, v. 352, p. 701–704, doi:10.1126/science.aaf2349.

Williams, C.A., Eberhart-Phillips, D., Bannister, S., Barker, D.H.N., Henrys, S., Reyners, M., and Sutherland, R., 2013, Revised Interface Geometry for the Hikurangi Subduction Zone, New Zealand: Seismological Research Letters, v. 84, p. 1066–1073, doi:10.1785/0220130035.

FIGURES AND TABLES

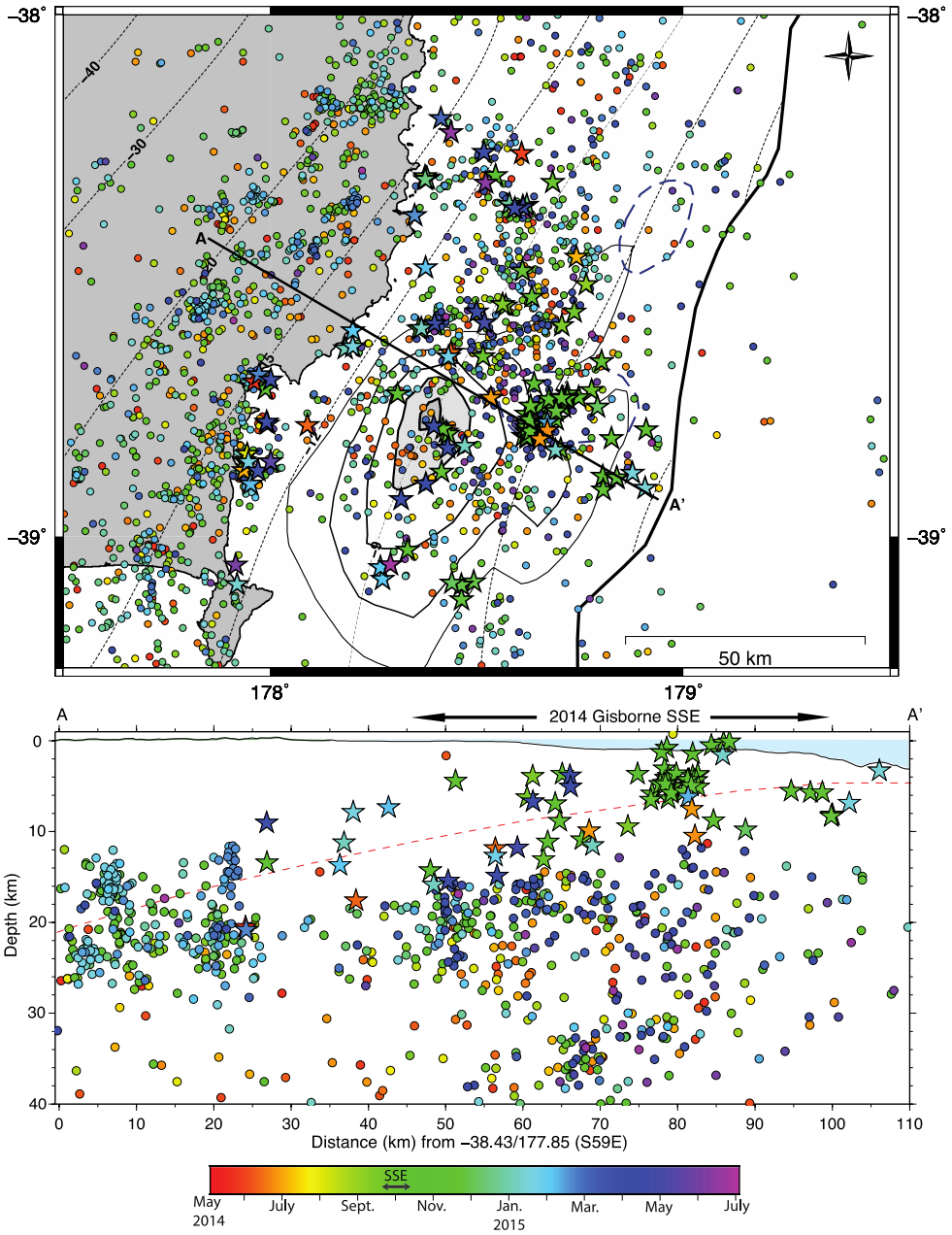

Figure DR1. Map and cross-section of seismicity (within 25 km of A-A') from May 2014 – June 2015. Locations are GrowClust relocations, or J. Yarce (personal communication, 2018) and Todd et al. (2018) initial locations for events that could not be relocated with GrowClust (see Figure DR2 for events relocated with GrowClust). General seismicity shown as circles, colored according to time. Earthquakes used as templates in this study are shown as stars, colored according to time. Plate interface contours (top: black dashed lines; bottom: red dashed line) from Williams et al., 2013. Slow slip event contours (black lines; mm slow slip) from Wallace et al., 2016.

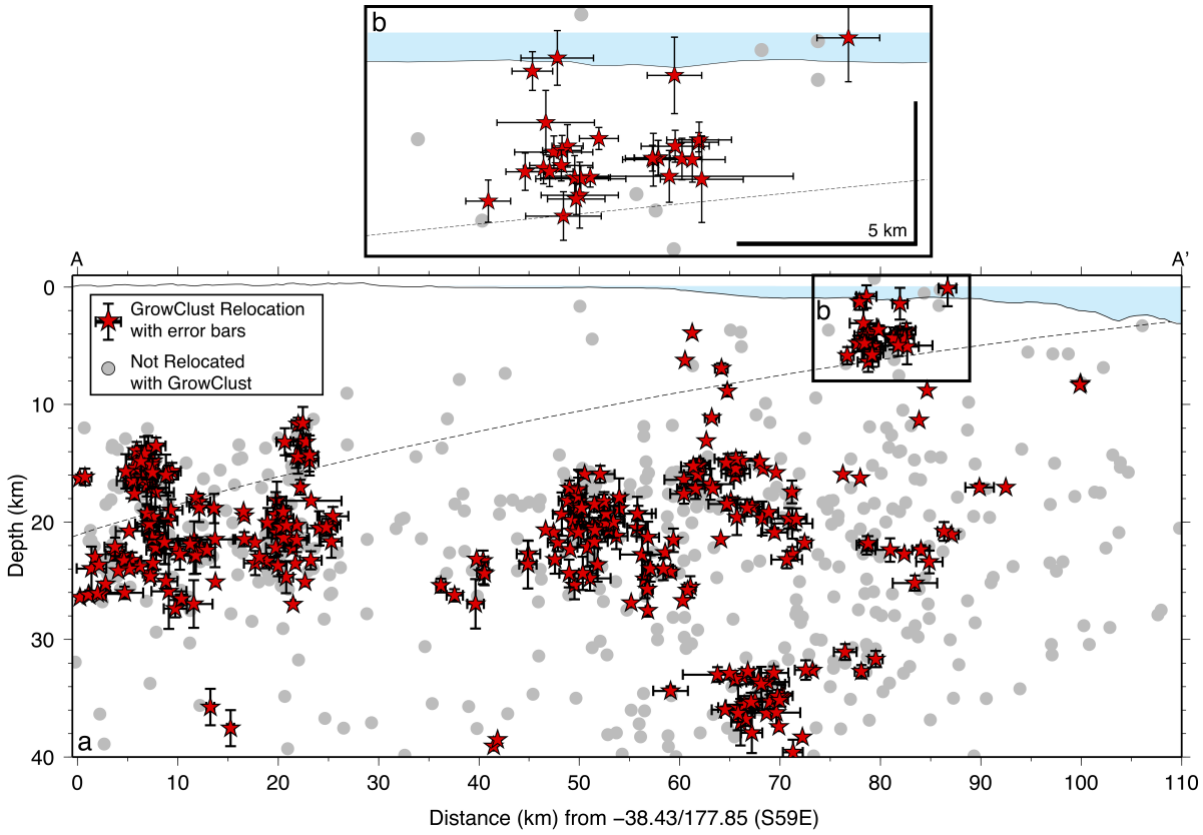

Figure DR2. a) Cross-section of seismicity (within 25 km of A-A' shown on Fig. DR1) from May 2014 – June 2015. Red stars: GrowClust relocations with vertical and horizontal error bars. Gray circles: events not relocated with GrowClust, locations are from J. Yarce (personal communication, 2018) or Todd et al. (2018) catalogs. Plate interface (black dashed line) from Williams et al., 2013. b) Zoom-in of upper plate seismicity with GrowClust error bars where "burst-type" repeating earthquakes are found.

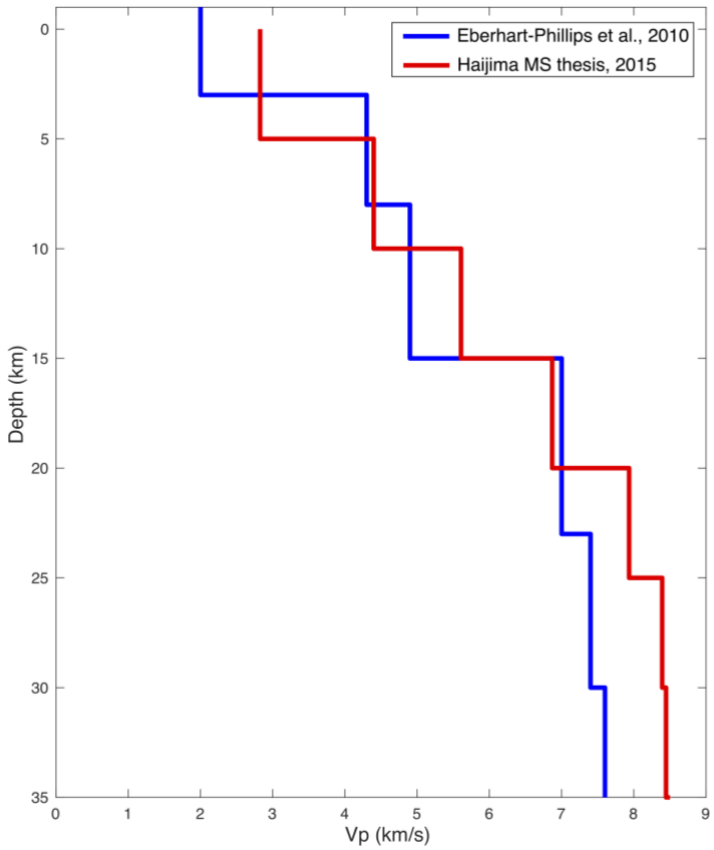

Figure DR3. Offshore 1-D interpretation of Eberhart-Phillips et al. (2010) 3-D seismic velocity model used in this study for GrowClust relocations, compared to the 1-D seismic velocity model near the subducted seamount from Haijima, D. MS thesis (2015) that used ocean-bottom seismometer data.

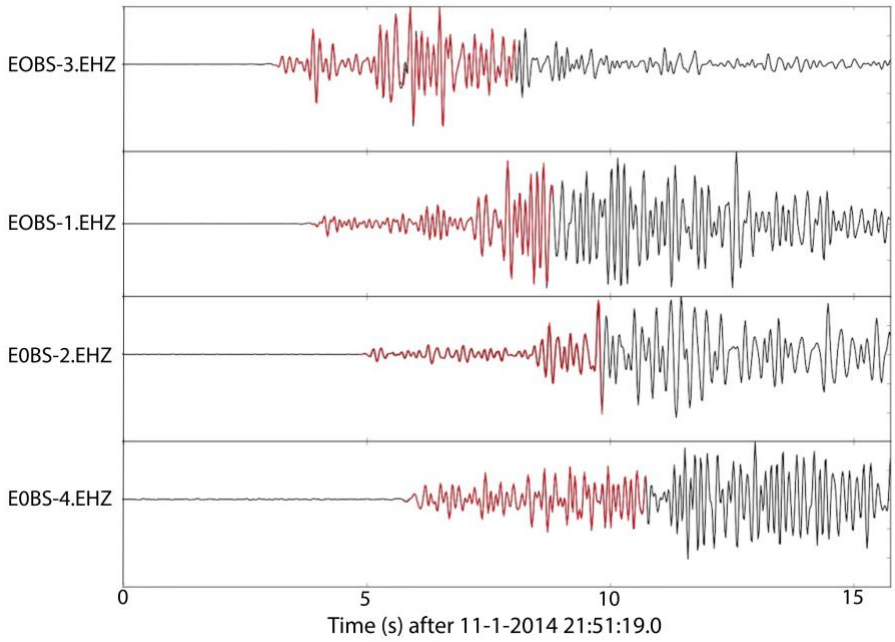

Figure DR4. Example "burst-type" repeating earthquake seismogram, average CC of 0.96. Template earthquake (Family ID 5, M_L 0.70, 2 events in family) shown in red (5s long around P-phase) occurred on 10-22-2014 at 15:54:34.44 UTC (at subducted seamount). Background waveform/detection shown in black. Vertical component, 3-10 Hz bandpass filtered waveforms shown. Traces normalized by maximum amplitude.

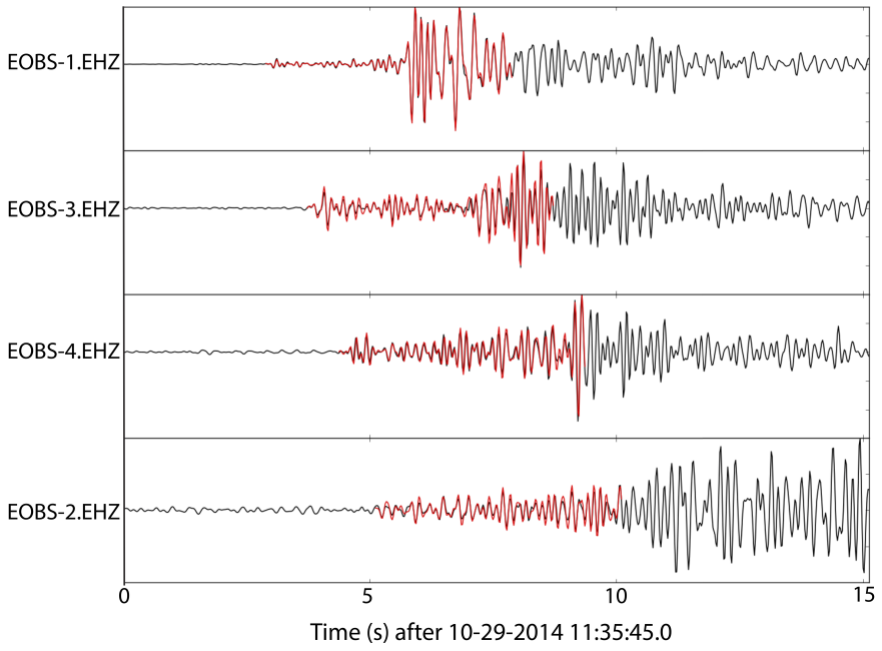

Figure DR5. Example "burst-type" repeating earthquake seismogram, average CC of 0.95. Template earthquake (Family ID 8, M_L 0.46, 2 events in family) shown in red (5s long around P-phase) occurred on 10-29-2014 at 17:02:15.38 UTC (at subducted seamount). Background waveform/detection shown in black. Vertical component, 3-10 Hz bandpass filtered waveforms shown. Traces normalized by maximum amplitude.

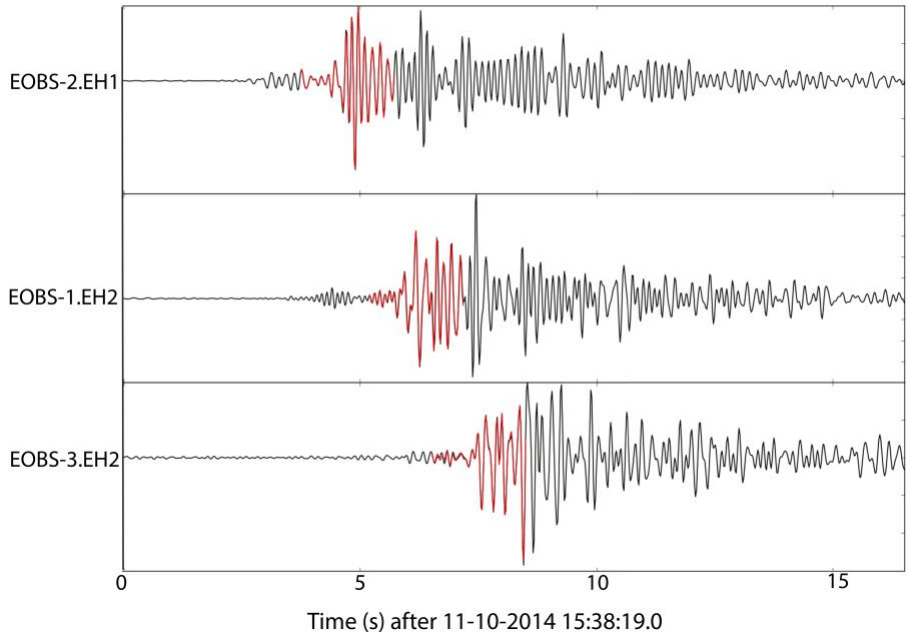

Figure DR6. Example "burst-type" repeating earthquake seismogram, average CC of 0.99. Template earthquake (Family ID 4, M_L 0.31, 7 events in family) shown in red (2s long around S-phase) occurred on 10-18-2014 at 16:44:01.64 UTC (at subducted seamount). Background waveform/detection shown in black. Horizontal components, 3-10 Hz bandpass filtered waveforms shown. Traces normalized by maximum amplitude.

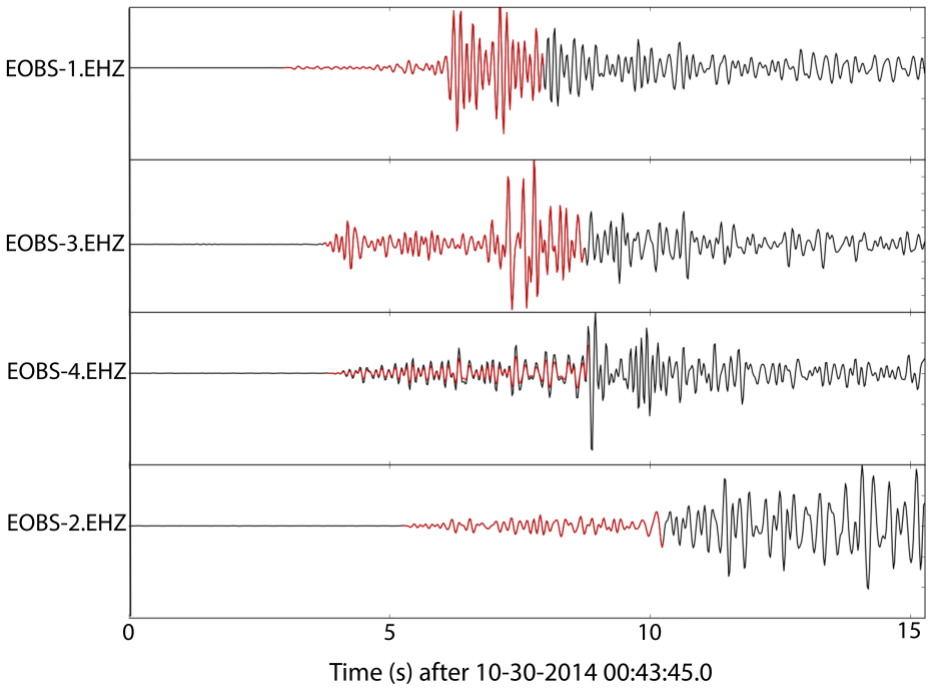

Figure DR7. Example "burst-type" repeating earthquake seismogram, average CC of 0.95. Template earthquake (Family ID 9, M_L 0.25, 5 events in family) shown in red (5s long around P-phase) occurred on 10-29-2014 at 22:17:49.16 UTC (at subducted seamount). Background waveform/detection shown in black. Vertical component, 3-10 Hz bandpass filtered waveforms shown. Traces normalized by maximum amplitude.

Table DR1. "Burst-Type" Repeating Earthquakes at Subducted Seamount

Family ID: 4, Template Time: 10-18-2014T16:44:01.64, Latitude: -38.7867, Longitude: 178.6311, Depth (km): 0.809, M_L: 0.31

Detection Time (UTC)	Average CC	# Stations	Template Type	M_L
10-09-2014T14:07:55	0.97	3	S-phase	-0.81
10-10-2014T07:54:49	0.97	3	S-phase	-0.97
10-15 -2014T13:29:47	0.97	3	S-phase	-1.18
10-15-2014T15:25:51	0.97	3	S-phase	-0.56
10-24-2014T20:00:29	0.97	3	S-phase	-0.42
11-10-2014T15:38:22	0.99	3	S-phase	0.05
10-18-2014T16:44:01	1	3	S-phase	0.31

Family ID: 5, Template Time: 10-22-2014T15:54:34.44, Latitude: -38.7088, Longitude: 178.6390, Depth (km): 3.66, M_L: 0.70

Detection Time (UTC)	Average CC	# Stations	Template Type	M_L
11-01-2014T21:51:22	0.96	4	P-phase	0.74
10-22-2014T15:54:34	1	4	P-phase	0.70

Family ID: 6, Template Time: 10-24-2014T00:33:43.98, Latitude: -38.7504, Longitude: 178.6561, Depth (km): 4.80, M_L: N/A

Detection Time (UTC)	Average CC	# Stations	Template Type	M_L
10-24-2014T00:38:53	0.95	4	P-phase	N/A
10-24-2014T00:33:43	1	4	P-phase	N/A

Family ID: 8, Template Time: 10-29-2014T17:02:15.38, Latitude: -38.7355, Longitude: 178.7082, Depth (km): 4.33, M_L: 0.46

Detection Time (UTC)	Average CC	# Stations	Template Type	M_L
10-29-2014T11:35:47	0.95	4	P-phase	0.19
10-29-2014T17:02:15	1	4	P-phase	0.46

Family ID: 9, Template Time: 10-29-2014T22:17:49.16, Latitude: -38.7280, Longitude: 178.7199, Depth (km): 1.42, M_L: 0.25

Detection Time (UTC)	Average CC	# Stations	Template Type	M_L
10-29-2014T22:14:02	0.97	4	P-phase	-0.61
10-29-2014T22:28:27	0.95	4	P-phase	-0.58
10-30-2014T00:43:47	0.95	4	P-phase	0.29
11-02-2014T08:05:22	0.95	4	P-phase	0.41
10-29-2014T22:17:49	1	4	P-phase	0.25

Family ID: 10, Template Time: 10-27-2014T14:03:45.68, Latitude: -38.7349, Longitude: 178.7470, Depth (km): 0.530, M_L: 0.60

Detection Time (UTC)	Average CC	# Stations	Template Type	M_L
10-27-2014T19:52:52	0.95	4	P-phase	0.10
10-27-2014T14:03:45	1	4	P-phase	0.60

Family ID: 11, Template Time: 10-28-2014T22:27:09.54, Latitude: -38.7386, Longitude: 178.6751, Depth (km): 5.76, M_L: 0.01

Detection Time (UTC)	Average CC	# Stations	Template Type	M_L
10-28-2014T22:25:09	0.96	4	P-phase	-1.07
10-28-2014T22:27:09	1	4	P-phase	0.01

Family ID: 13, Template Time: 11-08-2014T13:34:39.90, Latitude: -38.7775, Longitude: 178.6920, Depth (km): 5.07, M_L: 0.27

Detection Time (UTC)	Average CC	# Stations	Template Type	M_L
11-08-2014T11:44:39	0.96	4	S-phase	-0.88
11-08-2014T13:34:39	1	4	S-phase	0.27

Family ID: 14, Template Time: 11-14-2014T22:36:57.92, Latitude: -38.7514, Longitude: 178.6300, Depth (km): 6.52, M_L: 1.27

Detection Time (UTC)	Average CC	# Stations	Template Type	M_L
11-01-2014T09:28:02	0.96	3	S-phase	0.83
11-14-2014T22:36:57	1	3	S-phase	1.27

Family ID: 16, Template Time: 11-16-2014T19:57:17.72, Latitude: -38.7822, Longitude: 178.6640, Depth (km): 5.59, M_L: 1.35

Detection Time (UTC)	Average CC	# Stations	Template Type	M_L
11-05-2014T00:18:46	0.95	4	P-phase	0.23
11-16-2014T19:57:17	1	4	P-phase	1.35

Family ID: 17, Template Time: 12-01-2014T03:33:56.98, Latitude: -38.7532, Longitude: 178.7920, Depth (km): 9.81, M_L: 1.60

Detection Time (UTC)	Average CC	# Stations	Template Type	M_L
11-30-2014T03:29:53	0.99	3	P-phase	1.25
11-30-2014T03:28:32	0.95	3	S-phase	0.02
12-01-2014T03:33:56	1	3	P-phase/S-phase	1.60

P-phase: 5 seconds around P-phase arrival (0.15s pre-pick); S-phase: 2 seconds around S-phase arrival (1s pre-pick)
Template times are in UTC. Average CC = 1 is a template event.